ACS APPLIED MATERIALS & INTERFACES

Letter

www.acsami.org

Ultrathin $MoSe_2$ Nanosheets Decorated on Carbon Fiber Cloth as Binder-Free and High-Performance Electrocatalyst for Hydrogen Evolution

Bin Qu,[†,‡] Xianbo Yu,[†] Yujin Chen,[*,†] Chunling Zhu,[*,§] Chunyan Li,[*,†] Zhuoxun Yin,[†] and Xitian Zhang[#]

[†]Key Laboratory of In-Fiber Integrated Optics, Ministry of Education, and College of Science, [§]College of Material Science and Chemical EngineeringHarbin Engineering University, Harbin 150001, China

[‡]Department of Applied Chemistry, College of Science, Northeast Agricultural University, Harbin 150030, China

[#]Key Laboratory for Photonic and Electronic Bandgap Materials, Ministry of Education, and School of Physics and Electronic Engineering, Harbin Normal University, Harbin 150025, China

Supporting Information

ABSTRACT: $MoSe_2$ nanosheets with ultrathin thickness and rich defects were grown on the surface of carbon fiber cloth by a facile solvent-thermal method. The active area and conductivity of the $MoSe_2$ catalyst were increased simultaneously because of the NH_4F etching effect and its incorporation with carbon fiber cloth. As a result, the $MoSe_2$-based catalysts exhibited excellent HER activity including small onset potential, large exchange current density and small Tafel slope, which is superior to most of $MoSe_2$-based catalysts reported previously.

KEYWORDS: *hydrogen evolution, NH_4F etching effect, carbon fiber cloth, $MoSe_2$ nanosheets, catalysts*

Hydrogen, as a clean fuel, is a very promising candidate for traditional fossil fuels in the future. Electrochemical water splitting is one of efficient pathways to generate hydrogen.[1−4] To realize efficient water splitting, active catalysts for the hydrogen evolution reaction (HER) are needed. Although precious metals such as platinum exhibit good HER activity, their high cost and scarcity limit their large scale applications.[1−4] Recently, two-dimensional (2D) layered metal chalcogenide materials including MoS_2,[5−19] $MoSe_2$,[18−22] WS_2,[19,23] and WSe_2[19] have been reported as electrocatalysts for HER.[5−14] Among these 2D layered materials, MoS_2 has drawn wide attention because of its low cost, high chemical stability, and excellent electrocatalytic performance.[5−19] Both experimental and computational studies demonstrated that the electrocatalytic HER activity of MoS_2 depended strongly on the number of the active edge sites, whereas the basal surfaces were catalytically inert.[2,5,10,16,17] Therefore, various strategies including template-assistant route,[10] hydrothermal method,[7,16] and chemical vapor deposition,[18,19] have been developed to fabricate nanostructured MoS_2 with more exposed edge sites. The number of active sites of 2D layered MoS_2 materials has been significantly increased by these strategies, leading to a distinct enhancement of their HER activities. Because of the similarity of the $MoSe_2$ structure to that of MoS_2, the HER catalytic activity of $MoSe_2$ can also be improved significantly by reducing the $MoSe_2$ size down to nanoscale. For example, Cui's group has grown vertically aligned $MoSe_2$ molecular layers on flat substrates and even on curved and rough Si nanowires through a rapid vapor diffusion method.[18,19] The vertically aligned $MoSe_2$ molecular layers with respect to the substrates possessed maximally exposed active edge sites, and thereby exhibited large exchange current densities in HER.[18,19] Zhou et al. developed a bottom-up colloidal synthetic route to fabricate robust hierarchical ultrathin $MoSe_2{-}x$ nanosheets.[20] The $MoSe_2{-}x$ nanosheets had a thickness in the range of 1.3−2.6 nm, leading to their very good HER activities with a small onset potential and large cathodic current densities.[20]

Besides the aspect of the number of active edge sites, the electrical conductivity of 2D layered metal chalcogenide nanostructures plays an important role in their HER performance. However, the extremely low conductivity between two adjacent van der Waals bonded layers would significantly suppress their overall HER rate.[24] Deposition of 2D layered metal chalcogenide nanostructures on conductive substrates

Received: March 30, 2015
Accepted: June 25, 2015
Published: June 25, 2015

DOI: 10.1021/acsami.5b02753
ACS Appl. Mater. Interfaces 2015, 7, 14170−14175

such as carbon fiber paper, F-doped tin oxide glass and Ti foils could decrease their resistances to some degree.[8,14,21,25] However, most of the stacked layers are paralleled to the conductive substrates, limiting the charge transport efficiency along the adjacent edges from the conductive substrate to the active sites.[8,14,21,25] One efficient pathway to overcome the drawback is to fabricate 2D metal chalcogenide nanostructures with a few layers.[7,17,20] Another one is to orient them with the stacked layers perpendicular to the conductive substrates.[18,19] Nevertheless, the facile one-pot method, which aim to increase both the number of active edge sites and conductivity of the 2D layered materials such as $MoSe_2$ simultaneously, have rarely been reported.[18,19,26]

Recently, we grew MoS_2 nanosheet arrays on the surface of carbon fiber cloth (CFC) by a hydrothermal method.[26] Due to NH_4F etching effect and the incorporation of CFC, both the number of active edge sites and the conductivity of MoS_2 nanosheets were increased simultaneously, and thereby MoS_2 nanosheets exhibited enhanced catalytic activity to HER.[26] Because $MoSe_2$ has a very similar crystal structure to MoS_2, its HER activity may be improved by the same strategy as that utilized to MoS_2. However, the precursors for the synthesis of $MoSe_2$ are quite different from those for MoS_2. Therefore, it is necessary to exploit an appropriate method to synthesize $MoSe_2$ with highly catalytic activity to HER. Herein we develop a facile one-pot solvent-thermal method, in which MoO_3 powder and hydrazine hydrate−Se were used as precursors with an additive of NH_4F (Supporting Information), to grow $MoSe_2$ nanosheet arrays on the surface of carbon fiber cloth substrate. Experimental results showed that the density of $MoSe_2$ nanosheets on the surface of the carbon fibers can be controlled by tuning the synthetic conditions. Due to the NH_4F etching effect, some pits can be formed in the catalytically inert basal planes of the $MoSe_2$ nanosheets, leading to the increase in the numbers of active edge sites of our $MoSe_2$-based catalysts. As a result, the $MoSe_2$-based catalysts exhibited excellent HER activity including small onset potential, large exchange current density and small Tafel slope, which is superior to most of $MoSe_2$-based catalysts reported previously. Moreover, compared experiments in which the CFC was not added to the reaction system were conducted to investigate the growth process of $MoSe_2$ nanosheets and the NH_4F etching process. The results revealed that the etching method may be extended to synthesize other 2D layered metal chalcogenide materials with more exposed edge active sites for high-performance catalysts.

The samples, which were obtained at 220 °C for 6, 9, and 12 h, were named as CMSF-6, CMSF-9, and CMSF-12, respectively. For comparison, the sample obtained under the same conditions as those of CMSF-9 without NH_4F was named as CMS-9. Figure $1a_1$−a_4, b_1−b_4, c_1−c_4, and d_1−d_4 shows scanning electron microscopy (SEM) images of CMSF-6, CMSF-9, CMSF-12, and CMS-9 with different magnifications, respectively. The composites have similar ordered woven structures to that of the bare carbon fiber cloth, as shown in low-magnification SEM images (Figure $1a_1$−d_1). Even after a strong ultrasoniction, the $MoSe_2$ nanosheets were still attached on the surface of carbon fibers. It suggests a strong interaction between $MoSe_2$ nanosheets and the carbon fibers, benefiting the charge transfer between them during HER process. From Figure $1a_2$−c_2, it can be found that the $MoSe_2$ nanosheets are grown on the surface of carbon fibers in CMSF-6, CMSF-9, and CMSF-12 samples. It should be noted that a long reaction time would lead to small amount of spheres on the surface of carbon fibers (CMSF-12), which will suppress HER activity of the catalyst.

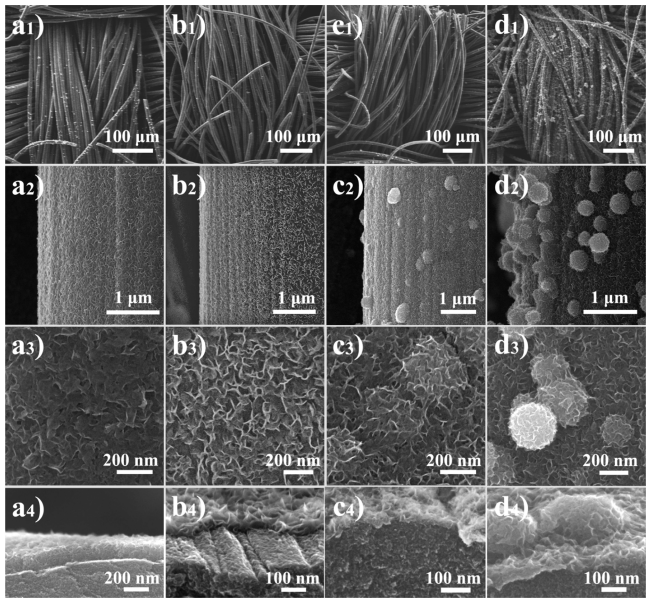

Figure 1. Typical SEM images of $MoSe_2$-based catalysts with different magnifications. (a_1−a_4) CMSF-6, (b_1−b_4) CMSF-9, (c_1−c_4) CMSF-12, and (d_1−d_4) CMS-9.

Figure $1a_3$−c_3 highlights that the nanosheets in CMSF-6, CMSF-9, and CMSF-12 samples have uniform lateral sizes in the range of 50−160 nm. The obvious ripples and corrugations can be observed in the SEM images, suggesting the ultrathin nature of the $MoSe_2$ nanosheets. Figure $1a_4$−c_4 shows cross-section SEM images of CMSF-6, CMSF-9, and CMSF-12, respectively. It can be found that if NH_4F is absent in the reaction system, besides nanosheets there are many dense and large spheres with an average diameter of 300 nm loaded on the surface of carbon fibers. This demonstrates that NH_4F in the solvent-thermal reaction system can efficiently impede overgrowth of $MoSe_2$ on carbon fibers to form larger $MoSe_2$ spheres, which originates from the NH_4F effect.

The morphology and the structure of the composites were further characterized by transmission electron microscopy (TEM) observations. Low-magnification TEM images (Figure $2a_1$−c_1) show that the thicknesses of the $MoSe_2$ nanosheets in CMSF-6, CMSF-9, and CMSF-12 are less than 7 nm. High-magnification TEM images (Figure $2a_2$−c_2) reveal that $MoSe_2$ nanosheets have a lamellar structure with a large number of exposed edge sites of the (002) plane. From the curled edge of the $MoSe_2$ nanosheets, there are typically about 5−6 Se−Mo−Se atomic layers. Importantly, $MoSe_2$ nanosheets in the rims of the basal planes have a thickness of 1−2 Se−Mo−Se atomic layers, indicative of the white arrows in the TEM images (Figure $2a_2$−c_2). The selected-area electron diffraction (SAED) patterns in the insets of Figure $2a_1$−c_1 and high-resolution TEM (HRTEM) images in Figure $2a_3$−c_3 demonstrate weak crystallinities of the $MoSe_2$ nanosheets in CMSF-6, CMSF-9 and CMSF-12. Furthermore, some pits are formed in the basal plane of the $MoSe_2$ nanosheets, highlighted in Figure S1 in the Supporting Information. The pits lead to more stacking faults and plane defects, and thereby result in additional edge sites that facilitate the enhancement of HER activity of the $MoSe_2$ nanosheets.[16]

DOI: 10.1021/acsami.5b02753
ACS Appl. Mater. Interfaces 2015, 7, 14170−14175

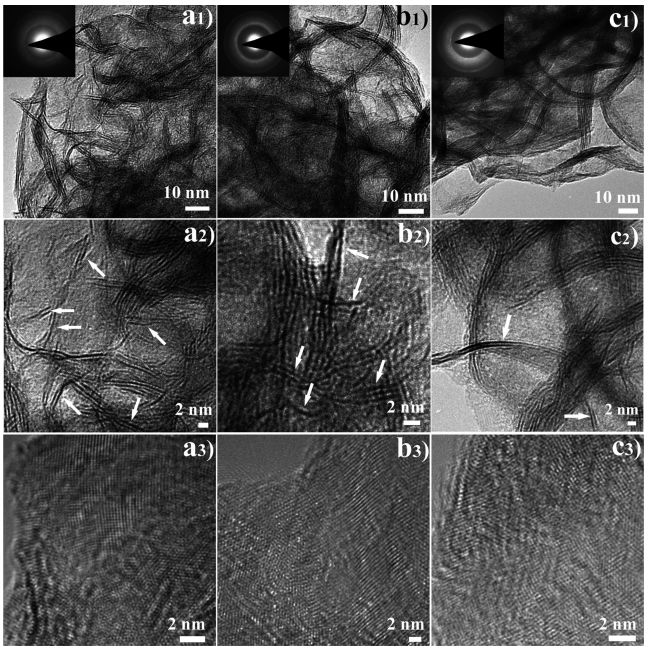

Figure 2. TEM images of $MoSe_2$-based catalysts. (a_1−a_3) CMSF-6, (b_1−b_3) CMSF-9, and (c_1−c_3) CMSF-12.

The SEM and TEM observations show that NH_4F can etch the $MoSe_2$ nanosheets. In order to further investigate the NH_4F etching process and the growth process of $MoSe_2$ nanosheets, compared experiments were conducted in which the carbon fiber cloth was not added to the reaction system. SEM and low-magnification TEM images (Figure S2a_1, a_2 in the Supporting Information) show that solid $MoSe_2$ spheres are obtained as the reaction time reaches 6 h. The lateral size of $MoSe_2$ nanosheets at the surface of the spheres is less than 50 nm, as shown in the high-magnification TEM image (Figure S2a_3 in the Supporting Information). SAED pattern (the inset of Figure S2a_3 in the Supporting Information) reveals weak crystallinity of $MoSe_2$ nanosheets. As the reaction time prolongs to 9 h, most of solid spheres change to hollow ones, as shown in Figure S2b_2 and the inset of Figure S2b_1. SEM and high-magnification TEM images (Figure S2b_1, b_3 in the Supporting Information) show that the lateral size of $MoSe_2$ nanosheets at the outer surface of the hollow spheres is increased to 50−180 nm. Obvious diffraction rings are observed in the SAED pattern (in the inset of Figure S2b_3 in the Supporting Information), suggesting that the crystallinity of $MoSe_2$ nanosheets is improved significantly. However, in the case of the absence of NH_4F in the reaction system, most of solid $MoSe_2$ spheres are obtained (Figure S3, Supporting Information). This reveals that NH_4F plays a very important role in the formation of hollow $MoSe_2$ spheres, and provides an additional evidence for the NH_4F etching effect. When the reaction time is increased to 12 h, the crystallinity $MoSe_2$ nanosheets is kept unchanged, as shown in the inset of Figure S2c_3 in the Supporting Information. However, around 50% of hollow $MoSe_2$ spheres are broken, and transform to smaller solid ones, as shown in Figure S2c_1, c_2 in the Supporting Information. At the same time, the lateral size of $MoSe_2$ nanosheets is decreased (Figure S2c_3 in the Supporting Information). The results above demonstrate that the growth of $MoSe_2$ nanosheets is predominant during the initial stage of the solvent-thermal reaction (before 6 h), and with the increase in the reaction time the etching of NH_4F to the $MoSe_2$ nanosheets become a predominant process gradually. The NH_4F etching effect on other kinds of materials such as TiO_2 spheres has also been reported recently,[27] and thus it may be extended to more kinds of materials such as other 2D layered metal chalcogenide materials. In addition, hollow $MoSe_2$ spheres are easily obtained by only tuning the reaction time, which can be applied other electrochemical fields such as high-performance anode for lithium-ion battery.

Raman spectroscopy, a nondestructive tool for characterizing layered 2D metal chalcogenide materials, was employed to investigate the lattice dynamics of our $MoSe_2$-based catalysts. All the $MoSe_2$-based catalysts showed characteristic A_{1g} (out-of-plane) and E^1_{2g} (in-plane) Raman modes (Figure S4 in the Supporting Information) located at 237.0 and 283.8 cm $^{-1}$ respectively, confirming the formation of $MoSe_2$.[19] the peak intensity of A_{1g} is much higher than that of the E^1_{2g}, which may be attributed to the edge-terminated $MoSe_2$ sheets in the composites.[19]

To investigate the chemical composition of the samples, X-ray photoelectron spectra (XPS) were carried out. Figure 3

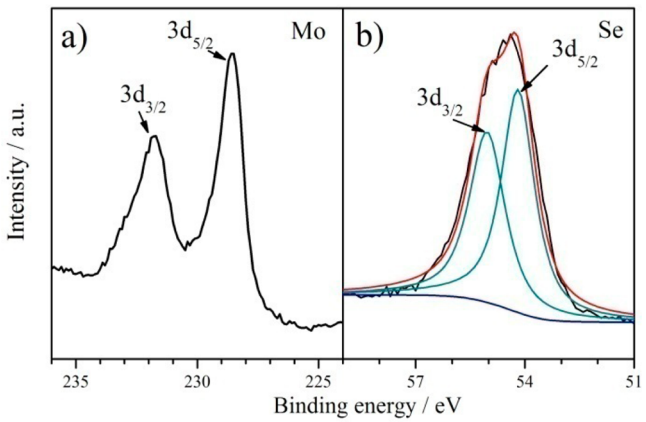

Figure 3. (a) Mo 3d and (b) Se 3d XPS spectra of CMSF-9.

shows Mo 3d and Se 3d spectra of CMSF-9. Two peaks which are located at 228.6 and 231.7 eV (Figure 3a) can be ascribed to Mo $3d_{5/2}$ and Mo $3d_{3/2}$, respectively, revealing that molybdenum is in its Mo(IV) state.[20−22,28] The binding energies at 54.4 and 55.3 eV arise from Se $3d_{5/2}$ and Se $3d_{3/2}$, respectively, suggesting the −2 oxidation state of Se in the nanosheets.[20−22] In addition, other samples synthesized in this work have similar XPS spectral features, as shown in Figure S5 in the Supporting Information. The compositional analysis results show that the atomic ratio of Mo to Se is in the range from 1:1.9 to 1:1.7, indicating that the surface of the nanosheets is Mo-rich with respect to stoichiometric of $MoSe_2$.

The SEM and TEM analyses demonstrate that ultrathin $MoSe_2$ nanosheet arrays can be uniformly grown on the surface of carbon fibers. The small thickness, rich defects on the basal plane, and incorporation with carbon fiber cloth suggest that our $MoSe_2$-based catalysts may have excellent HER performance. Electrochemical measurements of the $MoSe_2$-based catalysts and Pt were directly performed without any binders in 0.5 M H_2SO_4 solution using a three-electrode setup to investigate their HER activities. Figure 4a shows the polarization curves with a sweep rate of 3 mV s^{-1}. Pt catalyst exhibits expected HER activity with a near zero overpotential (η). All the $MoSe_2$-based composites exhibit a relatively high HER activity. Among these samples, CMSF-9 exhibits an onset

DOI: 10.1021/acsami.5b02753
ACS Appl. Mater. Interfaces 2015, 7, 14170−14175

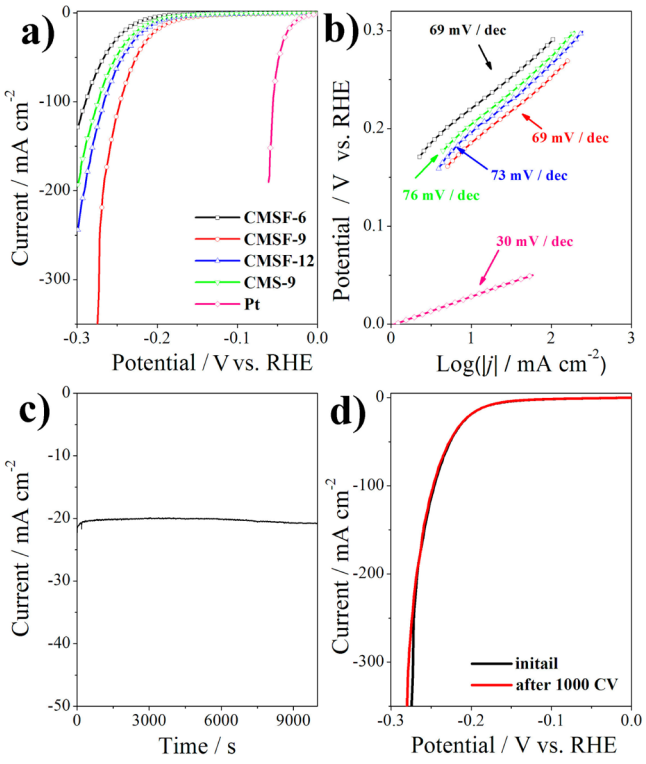

Figure 4. (a) Polarization curves of CMSF-6, CMSF-9, CMSF-12, CMS-9 and Pt; (b) Tafel plots of CMSF-6, CMSF-9, CMSF-12, CMS-9, and Pt; (c) cycling stability of CMSF-9 at an overpotential of 200 mV; and (d) the polarization curves before and after potential sweeps for 1000 cycles in 0.5 M H_2SO_4 solution.

potential (η) of 70 mV, smaller than those of CMSF-6 (145 mV), CMSF-12 (97 mV), and CMS-9 (115 mV). The cathodic current rises rapidly at more negative potentials for all the samples. Notably, CMSF-9 only requires an overpotential of 182 mV for driving a cathodic current density of 10 mA cm^{-2}, smaller than those of CMSF-6 (222 mV), CMSF-12 (198 mV), and CMS-9 (206 mV). This overpotential is also smaller than those of previously reported nanostructured $MoSe_2$ and $MoSe_2$-based composites (Table S1, Supporting Information),[18−22] which indicates superior catalytic activity of CMSF-9 for HER.

To further study of HER activity of the $MoSe_2$-based catalysts, Tafel plots were fitted to Tafel equation ($\eta = a + b\log j$), where b is the Tafel slope and j is the current density. As shown in Figure 4b, the Pt catalyst exhibits a Tafel slope of 30 mV dec^{-1}, which is consistent with the reported values. The Tafel slopes measured from these $MoSe_2$-based samples under small overpotential are in the range of 69−76 mV dec^{-1}, which suggests that the rate-determining step in HER mechanism on our $MoSe_2$-based catalysts may be the electrochemical desorption step (the Heyrovsky reaction).[10,29,30] The previous reports showed $MoSe_2$ catalysts had a large spread of Tafel slopes from 50−120 mV dec^{-1} (Table S1, Supporting Information).[18−22] The Tafel slopes of our catalysts are on the smaller side of this range, suggesting a faster increment of HER rate with a moderate increase of overpotential for our $MoSe_2$-based catalysts. Exchange current density (j_0) is another important parameter to evaluate the electrochemical performance of electrocatalysts, which represents intrinsic activities of electrocatalysts for the HER. By applying extrapolation method to the Tafel plots, exchange current densities for the $MoSe_2$-based catalysts can be obtained (Figure S6 and Table S1, Supporting Information). CMSF-9 and CMSF-12 exhibit larger exchange current densities of 21.1 and 23.3 μA cm^{-2} respectively, great larger than the values obtained for CMSF-6 (6.0 μA cm^{-2}) and CMS-9 (14.4 μA cm^{-2}). The exchange current densities are larger than those MoS_2-based catalysts,[16−18] further revealing the excellent activity of our $MoSe_2$-based catalysts toward HER.

From the results above, it can be found that CMSF-9 exhibits superior HER activities to other three catalysts. It may be related to the following factors. First, CMSF-9 has much larger active sites as compared to other samples. $MoSe_2$ nanosheet thin film in CMSF-6 is relatively denser, whereas there is many larger solid $MoSe_2$ spheres in CMS-9 samples. Therefore, the effective active areas of CMSF-6 and CMS-9 for HER are smaller than that of CMSF-9. As discussed above, there are small amount of $MoSe_2$ spheres in CMSF-12, which would result in the smaller active area of CMSF-12. The electrochemical double-layer capacitances (C_{dl}) can be measured to estimate the effective active area of our $MoSe_2$-based catalysts by using a simple cyclic voltammetry method (Figure S7, Supporting Information).[9] As shown in Figure S7e in the Supporting Information , CMSF-9 exhibits the C_{dl} value of 73.5 mF, greatly larger than CMSF-12 (25.0 mF), CMSF-6 (24.4 mF), and CMS-9 (19.5 mF). This result reveals that CMSF-9 has the largest effective active area among the $MoSe_2$-based catalysts, which contributes to its superior HER activity. Besides, the numbers of active sites of the samples were estimated in phosphate buffer solution (pH 7.0) according to a method previously reported.[12] Figure S8 in Supporting Information shows the cyclic voltammograms (CV) in the region of −0.2 to 0.6 V vs. RHE for our $MoSe_2$-based catalysts at pH 7.0. In terms of CV data, the upper limit of active sites could be calculated. The calculated numbers of the active sites of CMSF-9 (5.8×10^{-7} mol cm^{-2}) are higher than those of CMSF-6 (2.4×10^{-7} mol cm^{-2}), CMSF-12 (4.3×10^{-7} mol cm^{-2}) and CMS-9 (1.8×10^{-7} mol cm^{-2}). Second, the electric conductivity is another key factor to affect the activity of the electrocatalysts. In order to extract the charge-transfer resistance (R_{ct}) during HER process, electrochemical impedance spectroscopy (EIS) measurements were conducted at different overpotentials (Figure S9, Supporting Information). A two time-constant model can be used to describe the HER behavior on the $MoSe_2$-based electrodes (the inset in Figure S9a, Supporting Information). According to the Nyquist plots and the corresponding equivalent circuit models, the values of R_{ct} at different overpotentials can be extracted, and the values are listed in Table S2 (Supporting Information). As shown in Table S2 (Supporting Information), CMSF-9 has the lowest R_{ct} values among the $MoSe_2$-based catalysts. Thus, the superior HER activities of CMSF-9 is attributed to both higher effective active sites and higher overall conductivity. In addition, the small series resistances (R_s < 1.7 Ω cm^{-2}) for all the samples are beneficial in practical applications (Table S3, Supporting Information).

To investigate the stability of our $MoSe_2$-based catalysts during HER process, we carried out a long-term cycling test and continuous HER at a given overpotential. Long-term cycling stability of CMSF-9 is first investigated by operating continuous cyclic voltammetry (CV). As an overpotential of 200 mV was applied, CMSF-9 exhibited a continuous HER behavior. After a period of 10 000 s, the cathodic current density displays almost no degradation, as shown in Figure 4c. In addition, negligible difference can be observed between the

DOI: 10.1021/acsami.5b02753
ACS Appl. Mater. Interfaces 2015, 7, 14170−14175

curves measured at the initial cycle and after 1000 CV cycle (Figure 4d), suggesting the excellent stability of CMSF-9 toward HER. The results show that our $MoSe_2$-based catalysts exhibit a good stability during a long-term HER process in an acidic solution.

In summary, a facile one-pot solvent-thermal method has been developed to vertically grow $MoSe_2$ nanosheet arrays on carbon fiber cloth. Because of the NH_4F etching effect $MoSe_2$ nanosheets have ultrathin thicknesses, and rich defects and some pits on the inert basal plane, which resulted in a very high active area of the $MoSe_2$-based catalysts. Importantly, vertical growth of $MoSe_2$ nanosheets could significantly decrease the charge transfer resistance of the $MoSe_2$-based catalysts during HER process because the charges could be transferred from highly conductive carbon fiber directly to active edge sites of each single layer of $MoSe_2$ nanosheets, and thus the charge transfer along adjacent stacked layers with an extremely high resistance is not necessary. Both high active area and high conductivity lead to excellent HER performance of the $MoSe_2$-based catalysts including small onset potential, large exchange current density and small Tafel slope. Furthermore, the $MoSe_2$-based catalysts exhibit a good stability during a long-term HER process. Our results demonstrate that the $MoSe_2$-based catalysts presented here are very promising for practical applications.

■ ASSOCIATED CONTENT

Supporting Information

Experimental details and Figures S1−S9. The Supporting Information is available free of charge on the ACS Publications website at DOI: 10.1021/acsami.5b02753.

■ AUTHOR INFORMATION

Corresponding Authors

*E-mail: chenyujin@hrbeu.edu.cn.
*E-mail: zhuchunling@hrbeu.edu.cn.
*E-mail: chunyanli@hrbeu.edu.cn.

Notes

The authors declare no competing financial interest.

■ ACKNOWLEDGMENTS

We thank the National Natural Science Foundation of China (Grants 51272050 and 21271053), the Innovation Foundation of Harbin City (2012RFXXG096), and also the 111 project (B13015) of Ministry Education of China to the Harbin Engineering University.

■ REFERENCES

(1) Xu, K.; Chen, P. Z.; Li, X. L.; Tong, Y.; Ding, H.; Wu, X. J.; Chu, W. S.; Peng, Z. M.; Wu, C. Z.; Xie, Y. Metallic Nickel Nitride Nanosheets Realizing Enhanced Electrochemical Water Oxidation. *J. Am. Chem. Soc.* **2015**, *137*, 4119−4225.

(2) Karunadasa, H. I.; Montalvo, E.; Sun, Y. J.; Majda, M.; Long, J. R.; Chang, C. J. A Molecular MoS_2 Edge Site Mimic for Catalytic Hydrogen Generation. *Science* **2012**, *335*, 698−702.

(3) Feng, F.; Wu, J. C.; Wu, C. Z.; Xie, Y. Regulating the Electrical Behaviors of 2D Inorganic Nanomaterials for Energy Applications. *Small* **2015**, *11*, 654−666.

(4) Norskov, J. K.; Christensen, C. H. Chemistry-Toward Efficient Hydrogen Production at Surfaces. *Science* **2006**, *312*, 1322−1323.

(5) Hinnemann, B.; Moses, P. G.; Bonde, J.; Jørgensen, K. P.; Nielsen, J. H.; Horch, S.; Chorkendorff, I.; Nørskov, J. K. Biomimetic Hydrogen Evolution: MoS_2 Nanoparticles as Catalyst for Hydrogen Evolution. *J. Am. Chem. Soc.* **2005**, *127*, 5308−5309.

(6) Jaramillo, T. F.; Jørgensen, K. P.; Bonde, J.; Nielsen, J. H.; Horch, S.; Chorkendorff, I. Identification of Active Edge Sites for Electrochemical H_2 Evolution Form MoS_2 Nanocatalysts. *Science* **2007**, *317*, 100−102.

(7) Li, Y. G.; Wang, H. L.; Xie, L. M.; Liang, Y. Y.; Hong, G. S.; Dai, H. J. MoS_2 Nanoparticles Grown on Graphene: An Advanced Catalyst for The Hydrogen Evolution Reaction. *J. Am. Chem. Soc.* **2011**, *133*, 7296−7299.

(8) Guo, Y. Q.; Xu, K.; Wu, C. Z.; Zhao, J. Y.; Xie, Y. Surface Chemical-Modification for Engineering the Intrinsic Physical Properties of Inorganic Two-Dimensional Nanomaterials. *Chem. Soc. Rev.* **2015**, *44*, 637−646.

(9) Merki, D.; Vrubel, H.; Rovelli, L.; Fierro, S.; Hu, X. L. Fe, Co, and Ni Ions Promote The Catalytic activity of Amorphous Molybdenum Sulfide Films for Hydrogen Evolution. *Chem. Sci.* **2012**, *3*, 2515−2525.

(10) Kibsgaard, J.; Chen, Z. B.; Reinecke, B. N.; Jaramillo, T. F. Engineering The Surface Structure of MoS_2 to Preferentially Expose Active Edge Sites for Electrocatalysis. *Nat. Mater.* **2012**, *11*, 963−969.

(11) Lukowski, M. A.; Daniel, A. S.; Meng, F.; Forticaux, A.; Li, L. S.; Jin, S. Enhanced Hydrogen Evolution Catalysis from Chemically Exfoliated Metallic MoS_2 Nanosheets. *J. Am. Chem. Soc.* **2013**, *135*, 10274−10277.

(12) Merki, D.; Fierro, S.; Vrubel, H.; Hu, X. L. Amorphous Molybdenum Sulfide Films as Catalysts for Electrochemical Hydrogen Production in Water. *Chem. Sci.* **2011**, *2*, 1262−1267.

(13) Chang, Y. H.; Lin, C. T.; Chen, T. Y.; Hsu, C. L.; Lee, Y. H.; Zhang, W. J.; Wei, K. H.; Li, L. J. Highly Efficient Electrocatalytic Hydrogen Production by MoS_x Grown on Graphene-Protected 3D Ni Foams. *Adv. Mater.* **2013**, *25*, 756−760.

(14) Merki, D.; Hu, X. L. Recent Developments of Molybdenum and Tungsten Sulfides As Hydrogen Evolution Catalysts. *Energy Environ. Sci.* **2011**, *4*, 3878−3888.

(15) Zhang, K.; Zhao, Y.; Zhang, S.; Yu, H. L.; Chen, Y. J.; Gao, P.; Zhu, C. L. MoS_2 Nanosheet/Mo_2C-Embedded N-doped Carbon Nanotubes: Synthesis and Electrocatalytic Hydrogen Evolution Performance. *J. Mater. Chem. A* **2014**, *2*, 18715−18719.

(16) Xie, J. F.; Zhang, H.; Li, S.; Wang, R. X.; Sun, X.; Zhou, M.; Zhou, J. F.; Lou, X. W.; Xie, Y. Defect-Rich MoS_2 Ultrathin Nanosheets with Additional Active Edge Sites for Enhanced Electrocatalytic Hydrogen Evolution. *Adv. Mater.* **2013**, *25*, 5807−5813.

(17) Xie, J. F.; Zhang, J. J.; Li, S.; Grote, F.; Zhang, X. D.; Zhang, H.; Wang, R. X.; Lei, Y.; Pan, B. C.; Xie, Y. Controllable Disorder Engineering in Oxygen-Incorporated MoS_2 Ultrathin Nanosheets for Efficient Hydrogen Evolution. *J. Am. Chem. Soc.* **2013**, *135*, 17881−17888.

(18) Kong, D.; Wang, H.; Cha, J. J.; Pasta, M.; Koski, K. J.; Yao, J.; Cui, Y. Synthesis of MoS_2 and $MoSe_2$ Films with Vertically Aligned Layers. *Nano Lett.* **2013**, *13*, 1341−1347.

(19) Wang, H. T.; Kong, D. S.; Johanes, P.; Cha, J. J.; Zheng, G. Y.; Yan, K.; Liu, N. A.; Cui, Y. $MoSe_2$ and WSe_2 Nanofilms with Vertically Aligned Molecular Layers on Curved and Rough Surfaces. *Nano Lett.* **2013**, *13*, 3426−3433.

(20) Zhou, X. L.; Jiang, J.; Ding, T.; Zhang, J. J.; Pan, B. C.; Zuo, J.; Yang, Q. Fast Colloidal Synthesis of Scalable Mo-rich Hierarchical Ultrathin $MoSe_{2-x}$ Nanosheets for High−Performance Hydrogen Evolution. *Nanoscale* **2014**, *6*, 11046−11051.

(21) Tang, H.; Dou, K. P.; Kaun, C. C.; Kuang, Q.; Yang, S. H. $MoSe_2$ Nanosheets and Their Graphene Hybrids: Synthesis, Characterization and Hydrogen Evolution Reaction Studies. *J. Mater. Chem. A* **2014**, *2*, 360−364.

(22) Xu, C.; Peng, S. I.; Tan, C. L.; Ang, H. X.; Tan, H. T.; Zhang, H.; Yan, Q. Y. Ultrathin S-doped $MoSe_2$ Nanosheets for Efficient Hydrogen Evolution. *J. Mater. Chem. A* **2014**, *2*, 5597−5601.

(23) Voiry, D.; Yamaguchi, H.; Li, J. W.; Silva, R.; Alves, D. C. B.; Fujita, T.; Chen, M. W.; Asefa, T.; Shenoy, V. B.; Eda, G.; Chhowalla, M. Enhanced Catalytic Activity in Strained Chemically Exfoliated WS_2 Nanosheets for Hhydrogen Evolution. *Nat. Mater.* **2013**, *12*, 850−855.

DOI: 10.1021/acsami.5b02753
ACS Appl. Mater. Interfaces 2015, 7, 14170−14175

(24) Laursen, A. B.; Kegnæs, S.; Dahl, S.; Chorkendorff, I. Molybdenum Sulfides—Efficient and Viable Materials for Electro— and Photoelectrocatalytic Hydrogen Evolution. *Energy Environ. Sci.* **2012**, *5*, 5577—5591.
(25) Yan, Y.; Xia, B. Y.; Xu, Z. C.; Wang, X. Recent Development of Molybdenum Sulfides as Advanced Electrocatalysts for Hydrogen Evolution Reaction. *ACS Catal.* **2014**, *4*, 1693—1705.
(26) Yu, H. L.; Yu, X. B.; Chen, Y. J.; Zhang, S.; Gao, P.; Li, C. Y. A Strategy to Synergistically Increase the Number of Active Edge Sites and the Conductivity of MoS_2 Nanosheets for Hydrogen Evolution. *Nanoscale* **2015**, *7*, 8731—8738.
(27) Yu, S. L.; Liu, B. C.; Wang, Q.; Gao, Y. X.; Shi, Y.; Feng, X.; An, X. T.; Liu, L. X.; Zhang, J. Ionic Liquid Assisted Chemical Strategy to TiO_2 Hollow Nanocube Assemblies with Surface-Fluorination and Nitridation and High Energy Crystal Facet Exposure for Enhanced Photocatalysis. *ACS Appl. Mater. Interfaces* **2014**, *6*, 10283—10295.
(28) Vrubel, H.; Merki, D.; Hu, X. L. Hydrogen Evolution Catalyzed by MoS_3 and MoS_2 Particles. *Energy Environ. Sci.* **2012**, *5*, 6136—6144.
(29) Merki, D.; Fierro, S.; Vrubel, H.; Hu, X. L. Amorphous Molybdenum Sulfide Films as Catalysts for Electrochemical Hydrogen Production in Water. *Chem. Sci.* **2011**, *2*, 1262—1267.
(30) Bonde, J.; Moses, P. G.; Jaramilo, T. F.; Norskov, J. K.; Chorkendorff, I. Hydrogen Evolution on Nano-Particulate Transition Metal Sulfides. *Faraday Discuss.* **2008**, *140*, 219—231.

DOI: 10.1021/acsami.5b02753
ACS Appl. Mater. Interfaces 2015, 7, 14170—14175